

KAUNAS UNIVERSITY OF TECHNOLOGY
VYTAUTAS MAGNUS UNIVERSITY
VILNIUS GEDIMINAS TECHNICAL UNIVERSITY

SANDRA ALEKSIENĖ

**HIDING VISUAL INFORMATION IN DEFORMABLE AND
TWO-DIMENSIONAL MOIRÉ GRATINGS**

Summary of Doctoral Dissertation
Physical Sciences, Informatics (09P)

2019, Kaunas

This doctoral dissertation was prepared at Kaunas University of Technology, Faculty of Mathematics and Natural Sciences, Department of Mathematical Modelling during the period of 2013–2018.

Scientific Supervisor:

Prof. Dr. Habil. Minvydas Kazys RAGULSKIS (Kaunas University of Technology, Physical Sciences, Informatics – 09P).

Editor: Dovilė Dumbrasuskaitė (Publishing Office “Technologija”)

Dissertation Defence Board of Informatics Science Field:

Prof. Dr. Habil. Rimantas BARAUSKAS (Kaunas University of Technology, Physical Sciences, Informatics – 09P) – **chairman**;

Prof. Dr. Habil. Raimondas ČIEGIS (Vilnius Gediminas Technical University, Physical Sciences, Informatics – 09P);

Prof. Dr. Vacius JUSAS (Kaunas University of Technology, Informatics – 09P);

Prof. Dr. Habil. Genadijus KULVIETIS (Vilnius Gediminas Technical University, Physical Sciences, Informatics – 09P);

Prof. Dr. Miguel A. F. SANJUAN (Rey Juan Carlos University, Physical Sciences, Informatics – 09P).

The official defence of the dissertation will be held at 10 a.m. on 14 March, 2019 at the public meeting of Dissertation Defence Board of Informatics Science Field in the Dissertation Defence Hall at Kaunas University of Technology.

Address: K. Donelaičio St. 73-403, 44249 Kaunas, Lithuania.

Tel. no. (+370) 37 300 042; fax. (+370) 37 324 144; e-mail doktorantura@ktu.lt.

Summary of doctoral dissertation was sent on 14 February, 2019.

The doctoral dissertation is available on the internet <http://ktu.edu> and at the libraries of Kaunas University of Technology (K. Donelaičio St. 20, 44239 Kaunas), Vytautas Magnus University (K. Donelaičio St. 52, 44244 Kaunas) and Vilnius Gediminas Technical University (Saulėtekio al. 14, 10223 Vilnius).

KAUNO TECHNOLOGIJOS UNIVERSITETAS
VYTAUTO DIDŽIOJO UNIVERSITETAS
VILNIAUS GEDIMINO TECHNIKOS UNIVERSITETAS

SANDRA ALEKSIENĖ

**VIZUALIOSIOS INFORMACIJOS SLĖPIMAS
DEFORMUOJAMOSIOSE BEI DVIMATĖSE MUARO
GARDELĖSE**

Daktaro disertacijos santrauka
Fiziniai mokslai, Informatika (09P)

2019, Kaunas

Disertacija rengta 2013–2018 metais Kauno technologijos universiteto Matematikos ir gamtos mokslų fakultete Matematinio modeliavimo katedroje.

Mokslinis vadovas:

Prof. habil. dr. Minvydas Kazys RAGULSKIS (Kauno technologijos universitetas, fiziniai mokslai, informatika – 09P).

Redagavo: Rozita Znamenskaitė (Leidykla „Technologija“).

Informatikos mokslo krypties disertacijos gynimo taryba:

Prof. habil. dr. Rimantas BARAUSKAS (Kauno technologijos universitetas, fiziniai mokslai, informatika – 09P) – **pirmininkas**;

Prof. habil. dr. Raimondas ČIEGIS (Vilniaus Gedimino technikos universitetas, fiziniai mokslai, informatika – 09P);

Prof. dr. Vacius JUSAS (Kauno technologijos universitetas, fiziniai mokslai, informatika – 09P);

Prof. habil. dr. Genadijus KULVIETIS (Vilniaus Gedimino technikos universitetas, fiziniai mokslai, informatika – 09P);

Prof. dr. Miguel A. F. SANJUAN (Rey Juan Carlos universitetas, fiziniai mokslai, informatika – 09P).

Disertacija bus ginama viešame Informatikos mokslo krypties disertacijos gynimo tarybos posėdyje 2019 m. kovo 14 d. 10 val. Kauno technologijos universiteto disertacijų gynimo salėje.

Adresas: K. Donelaičio g. 73-403, 44249 Kaunas, Lietuva.

Tel. (370) 37 300 042; faks. (370) 37 324 144; el. paštas doktorantura@ktu.lt.

Disertacijos santrauka išsiųsta 2019 m. vasario 14 d.

Su disertacija galima susipažinti internetinėje svetainėje <http://ktu.edu>, Kauno technologijos universiteto (K. Donelaičio g. 20, 44239 Kaunas), Vytauto Didžiojo universiteto (K. Donelaičio g. 52, 44244 Kaunas) ir Vilniaus Gedimino technikos universiteto (Saulėtekio al. 14, 10223 Vilnius) bibliotekose.

INTRODUCTION

Dynamic visual cryptography-based numerical image coding schemes can be applied to a variety of scientific and engineering tasks. The ability of the human visual system to average the images of fast-moving objects in time can be used to identify specific diseases of the visual system, identify human fatigue, and perform optical diagnostics of technical systems [1]. On the other hand, these secret image coding schemes have a rather large application potential in MOEMS (micro-opto-electromechanical systems) [2]. However, when forming an optical phase profile for CGH (computer-generated holograms), it is necessary to take into account that image oscillating in the projection plane is reflected from the deformable MOEMS element. Thus, all of the dynamic visual cryptographic algorithms that have been suggested so far are inappropriate when light flux is reflected from a deformable body surface. The aim of this dissertation is to create theoretical foundations and construct appropriate algorithms that allow the modeling of optical effects of dynamic visual cryptography in deformable and two-dimensional moiré gratings.

The object of the research

1. The development of dynamic visual cryptography-based numerical image hiding algorithms in deformable harmonic moiré gratings.
2. The development of dynamic visual cryptography-based numerical image hiding algorithms in deformable chaotic moiré gratings.
3. The development of dynamic visual cryptography-based numerical image hiding algorithms in two-dimensional cross-gratings.

The aim of the research

To develop dynamic visual cryptography-based numerical image hiding techniques in deformable and two-dimensional moiré gratings.

The objectives of the research

The following objectives have been set to achieve the aim of the research:

1. To construct a dynamic visual cryptography scheme in deformable moiré gratings and apply this scheme to hide images in the gratings described by finite elements.
2. To apply a scheme of dynamic visual cryptography based on hiding numerical images in the case of chaotic oscillations.
3. To construct a scheme for hiding numerical images in two-dimensional cross-gratings.
4. To construct a setup for the experimental verification of the presented numerical image hiding algorithms.

The methodology of the research

The objectives for defining the parameters of deformable two-dimensional stochastic moiré gratings, secret image coding and decoding algorithms are constructed and solved in MATLAB software environment. The problems of surface dynamics of the deformed bodies described by finite elements are solved with the help of COMSOL program. The optimal model parameters are determined using analytical methods.

Scientific novelty and practical significance of the work

1. New methods of dynamic visual cryptography have been proposed in the thesis, where a deformed moiré grating oscillates harmonically and chaotically according to a certain Eigen-shape. A detailed analysis of these new methods opens the possibilities of applying the proposed methods for optical control of micro-opto-electromechanical systems.
2. The most important element of the scientific novelty of this dissertation is the realization of dynamic visual cryptography in two-dimensional finite element gratings. In the works known so far, the principle of dynamic visual cryptography-based image hiding was based on the formation of time-averaged moiré fringe in one-dimensional moiré gratings. Applying image coding algorithms to two-dimensional gratings greatly expands the scope of the presented algorithms that constitutes the practical value of this dissertation.

The approbation of the work results

8 scientific articles have been published on the topic of the dissertation, including 4 articles in the journals of the Main List of the Institute of Scientific Information (ISI) with citation index, 3 articles have been presented in international scientific conferences and published in conference proceedings.

The structure of the dissertation

The dissertation consists of an introduction, three chapters, conclusions, a list of references and a list of publications. The volume of the dissertation is 92 pages. The main part of the dissertation consists of 66 figures and includes 98 references.

1. LITERATURE REVIEW

Geometric moiré is a classical in-plane optical experimental technique based on the investigation of visual patterns produced by the superposition of two regular gratings that geometrically interfere [3–5]. Moiré techniques are used to measure variables such as displacements, curvature, rotation, and tension in a given area.

Moiré effects are also applied in areas such as interferometry [6, 7], moiré deflectometry [8–11], moiré topography [12–14], steganography [15], fraud prevention [16], and microscopy [17, 18].

The scientific articles dealing with moiré fringes can be divided into three categories:

1. Targeted interfering moiré fringes with the aim of creating the desired pattern. As a typical example, the structures of the designer-made moiré patterned structures in architecture can be presented [19].
2. Moiré interference fringes appear as a side, undesirable phenomenon and ways to eliminate them are sought [20–22].
3. Deformations of the observed body are determined from the experimental studies of the moiré fringe images [23].

Visual cryptography is a cryptographic technique that allows to encrypt visual information (e.g. text, pictures, etc.) in such a way that decryption is only performed with the help of human visual system without any additional calculations. Naor and Shamir are considered to be the initiators of visual cryptography [24]. The classic visual cryptographic scheme is cryptographically rather secure because without all the shares it is impossible to restore the secret information. However, a lack of this scheme introduces major possibilities of fraud.

The technique of hiding the image, when the secret image appears in the form of time-averaged moiré fringes when the non-deformable encoded image oscillates, was first proposed in article [25]. Here, in order to hide the secret image in one encoded image, a stochastic moiré grating is employed. Secret information is decoded by the naked eye when the amplitude of the harmonic oscillations exactly matches the preset value. Although the encoded image is not cryptographically secure, by combining visual cryptography, the effect of the formation of the interference fringes, and the procedure of time-averaging, we obtain a new image hiding technique, i.e. dynamic visual cryptography [26, 27]. Unlike classic visual cryptography, where multiple shares put on top of each other are used to decode a secret image, only one share is used for dynamic visual cryptography, i.e. decoding is performed by oscillating the encoded image exactly according to a predefined trajectory. Since the dynamic visual cryptography technique can be applied to human vision system research, in micro-opto-electromechanical systems, it is essential to expand the research of this technique in deformable and two-dimensional moiré gratings.

2. A DEFORMABLE MOIRE GRATING

Two phases are important in dynamic visual cryptographic tasks: encoding and decoding. Each of these phases requires certain steps. The algorithms for coding and decoding are presented below.

The algorithm for encoding:

1. The selection of λ_b – pitch of the moiré grating for the background.
2. The selection of the law according to which the grating is oscillated.
3. The selection of the pitch for the secret information λ_s , solving the two-criteria optimization task.
4. The selection of the secret image.
5. The application of phase regularization and initial random phase algorithms for hiding the image in the stochastic moiré grating.

The algorithm for decoding:

1. The oscillation of the encoded image according to the given law for the recording of the time-averaged image.

The algorithm descriptions reveal that the coding phase is much more complex than the decoding phase.

2.1. Estimation of optimal pitch of a moiré grating in dynamic visual cryptography¹

The standard deviation of the time-averaged greyscale intensity can be calculated according to [28]:

$$S(F_t(x)) = \frac{\left| J_0\left(\frac{2\pi}{\lambda}a\right) \right|}{\sqrt{8}}. \quad (2.1)$$

Let the pitch of grating in the area of secret information be denoted by λ_s and the pitch of grating in the background – λ_b . The pitches of grating λ_s and λ_b cannot differ significantly $|\lambda_s - \lambda_b| \leq \varepsilon$, otherwise the encoded secret could be seen by a naked eye in a static share. Simultaneously, the difference between λ_s and λ_b should ensure a sufficient contrast between secret and background areas in the time-averaged image.

Let the standard deviations of the secret and background areas in the time-averaged image be denoted as σ_s and σ_b respectively. The values of σ_s and σ_b are calculated as [28]:

$$\sigma_s = \frac{\left| J_0\left(\frac{2\pi}{\lambda_s}a\right) \right|}{\sqrt{8}}, \quad \sigma_b = \frac{\left| J_0\left(\frac{2\pi}{\lambda_b}a\right) \right|}{\sqrt{8}}. \quad (2.2)$$

A sufficient contrast between the leaked secret and the background in the time-averaged cover image is obtained only if $|\sigma_s - \sigma_b| \geq \delta$. Thus, the objective function for optimization is $\max |\sigma_s - \sigma_b|$ with constraint $|\lambda_s - \lambda_b| \leq \varepsilon$. The graphical representation of standard deviations σ_s and σ_b is proposed in Fig. 2.1.

¹ *The results presented in this section have been published as:*

Near-optimal pitch of a moiré grating for image hiding applications in dynamic visual cryptography
 Saunoriene L.; Aleksiene S.; Ragulskiene J.
 Copyright © 2017 JVE International.

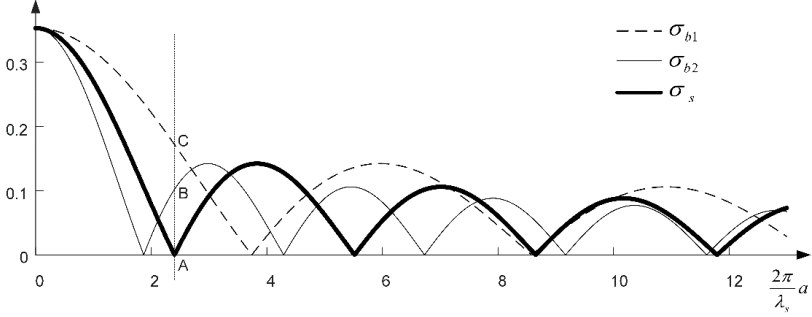


Fig. 2.1. The variation of standard deviations of a time-averaged moiré. The thick solid line stands for standard deviation of the secret σ_s at $\lambda_s = 0.45$; the thin solid and dashed lines represent standard deviations of the background σ_{b1} and σ_{b2} at $\lambda_{b1} = 0.7$, $\lambda_{b2} = 0.35$ accordingly

Let us assume that the contrast of the leaked secret in the time-averaged cover image is sufficient, if standard deviation σ_b is equal or exceeds threshold δ :

$$\left| \frac{J_0\left(\frac{2\pi a}{\lambda_b}\right)}{\sqrt{8}} \right| \geq \delta, \quad (2.3)$$

Whereas the amplitude of oscillation is preset to $a = \frac{\lambda}{2\pi} r_1$, Eq. (2.3) yields:

$$\left| \frac{J_0\left(\frac{\lambda_s r_1}{\lambda_b}\right)}{\sqrt{8}} \right| \geq \delta. \quad (2.4)$$

Inequality 2.4 is visualized in Fig. 2.2 when λ_s is fixed. Striped intervals on the graph show the intervals of λ_b for which inequality $\left| J_0\left(\frac{\lambda_s}{\lambda_b} r_1\right) \right| / \sqrt{8} \geq \delta$ holds true. Zeroes of the function $J_0\left(\frac{\lambda_s}{\lambda_b} r_1\right)$ are located at $\lambda_b = \lambda_s \frac{r_1}{r_i}$, $i = 1, 2, \dots$

To obtain a sufficient predetermined contrast between secret and background areas ($\sigma_b = \delta$), it would be optimal to choose such values of λ_b that lie on the contours of the grey and striped grey areas in Fig. 2.3, or, if δ is small, the approximate optimal solution is:

$$\lambda_b = \lambda_s \left(1 + \frac{\delta}{r_1 J_1(r_1)} \right) \text{ or } \lambda_b = \lambda_s \left(1 - \frac{\delta}{r_1 J_1(r_1)} \right). \quad (2.5)$$

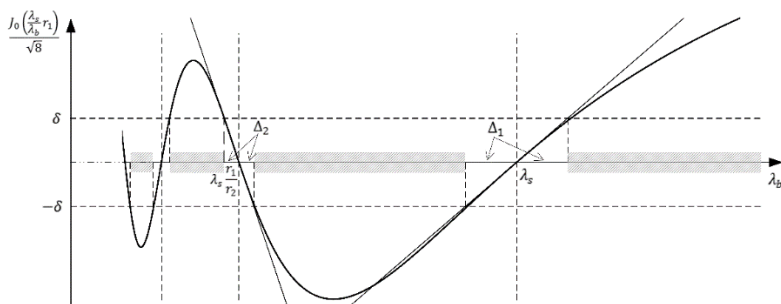


Fig. 2.2. Visualization of inequality $\left| \frac{J_0\left(\frac{\lambda_s r_1}{\lambda_b}\right)}{\sqrt{8}} \right| \geq \delta$ in the interval $(0.2\lambda_s; 1.5\lambda_s)$. The thick solid line represents the variation of $\left| \frac{J_0\left(\frac{\lambda_s r_1}{\lambda_b}\right)}{\sqrt{8}} \right|$; tangents at points λ_s and $\lambda_s \frac{r_1}{r_2}$ are displayed by thin lines

Note, that the difference between values λ_s and λ_b still should be small enough in order to ensure the safety of the visual encoding scheme.

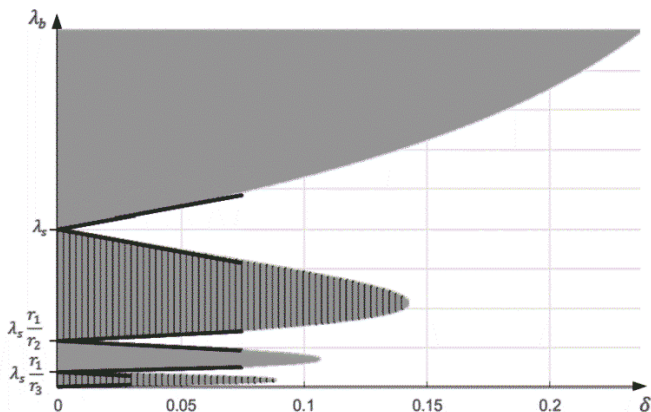


Fig. 2.3. Solutions of inequality $\left| \frac{J_0\left(\frac{\lambda_s r_1}{\lambda_b}\right)}{\sqrt{8}} \right| \geq \delta$: grey color indicates areas where $\frac{J_0\left(\frac{\lambda_s r_1}{\lambda_b}\right)}{\sqrt{8}} \geq \delta$, striped grey areas – where $\frac{J_0\left(\frac{\lambda_s r_1}{\lambda_b}\right)}{\sqrt{8}} \leq -\delta$, black lines correspond to the boundaries of the approximate solution

2.2. Harmonic oscillations, deformable moiré grating²

Let us consider a harmonic moiré grating on the surface of a one-dimensional deformable body. Let us assume that the deflection of point x from the state of equilibrium is $u(x, t)$. Then the deformed moiré grating reads [29]:

$$F(x, t) = \frac{1}{2} + \frac{1}{2} \cos\left(\frac{2\pi}{\lambda} \mu(x, t)\right), \quad (2.6)$$

only if the independent variable x can be expressed from the relationship

$$x + u(x, t) = z \quad (2.7)$$

into the explicit form

$$x = \mu(z, t). \quad (2.8)$$

Let us assume that the space and time variables can be separated in the deflection function $u(x, t)$:

$$u(x, t) = a(x) \cdot g(t), \quad (2.9)$$

where $a(x)$ is the shape function of in-plane oscillations; $g(t)$ is the time process.

Now let us linearize function $a(x)$ around the point $x = x_0$:

$$a(x) = a_0 + \dot{a}_0(x - x_0) + O((x - x_0)^2), \quad (2.10)$$

where $a_0 = a(x_0)$ and $\dot{a}_0 = \left. \frac{da(x)}{dx} \right|_{x=x_0}$. Equations (2.7), (2.9) and (2.10) yield the relationship:

$$x \approx \frac{z - (a_0 - \dot{a}_0 x_0)g(t)}{1 + \dot{a}_0 g(t)}. \quad (2.11)$$

Thus the deformed moiré grating reads:

$$F(x, t) \approx \frac{1}{2} + \frac{1}{2} \cos\left(\frac{2\pi}{\lambda} \cdot \frac{x - (a_0 - \dot{a}_0 x_0)g(t)}{1 + \dot{a}_0 g(t)}\right). \quad (2.12)$$

Averaging of Eq. (2.12) in time yields:

$$F_t(x) \approx \frac{1}{2} + \frac{1}{2} \lim_{T \rightarrow \infty} \frac{1}{T} \int_0^T \cos\left(\frac{2\pi}{\lambda} \cdot \frac{x - (a_0 - \dot{a}_0 x_0)g(t)}{1 + \dot{a}_0 g(t)}\right) dt. \quad (2.13)$$

If the deformation field is linear $a(x) = Ax$ [29], then time-averaging yields:

² The results presented in this section have been published as:

Optical image hiding based on chaotic vibration of deformable moiré grating

Lu G., Saunoriene L., Aleksiene S., Ragulskis M.

Copyright © 2018 Elsevier B.V.

$$F_t(x) \approx \frac{1}{2} + \frac{1}{2} \cos\left(\frac{2\pi}{\lambda}x\right) J_0\left(\frac{2\pi}{\lambda}Ax\right). \quad (2.14)$$

Thus, time-averaged moiré fringes do form at $\frac{2\pi}{\lambda}Ax = r_i$, $i = 1, 2, \dots$. Figure 2.4 illustrates the formation of time averaged moiré fringes for the deformable moiré grating.

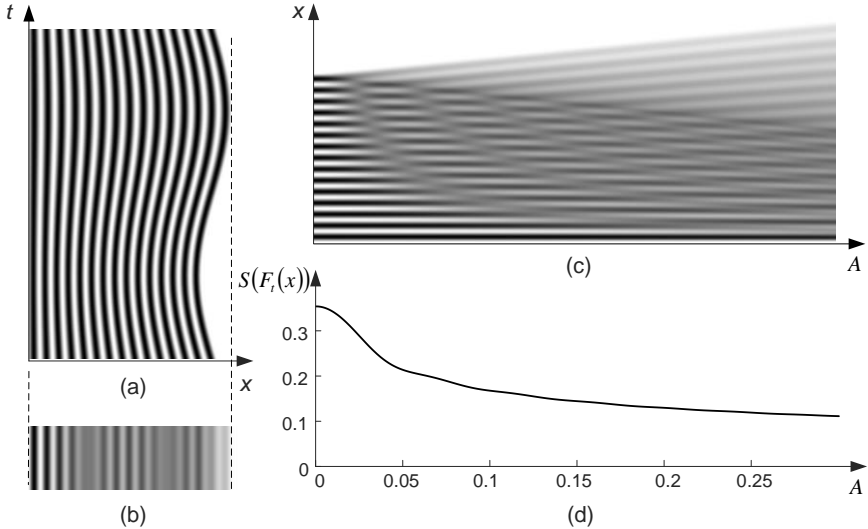


Fig. 2.4. Time-averaged image of the deformable one-dimensional moiré grating. The pitch of the grating in the state of equilibrium is $\lambda = 0.2$. (a) motion of one-dimensional moiré grating during one period of oscillations ($A = 0.075$; dashed line indicates maximum displacement from the state of equilibrium); (b) time-averaged image of part (a); (c) one-dimensional time-averaged moiré grating at increasing amplitudes A ; (d) standard deviation of the time-averaged image

The left side of the grating is fixed motionlessly, while the right side oscillates harmonically (amplitude A varies from 0 to 0.3 in the observation window). The pitch of the moiré grating at the state of equilibrium is $\lambda = 0.2$. Figure 2.4(a) illustrates the motion of one-dimensional deformable moiré grating during one period of oscillations. The time-averaged image of Figure 2.4(a) is presented in Figure 2.4(b), and Figure 2.4(c) shows the time-averaged one-dimensional moiré gratings at increasing amplitudes A (the higher is the amplitude of harmonic oscillations, the larger number of moiré fringes is visible in the time-averaged image).

2.3. Dynamic visual cryptography based on deformable moiré gratings on finite element grids³

A nonlinear field of deformation is used for the formation of time-averaged moiré fringes. The 2D field of deformations $a(x,y)$ constructed by FEM computations is sliced horizontally. One-dimensional pitch distributions are computed in adjacent moiré gratings. Therefore, every row of pixels in the digital image of 2D deformations is interpreted as a one-dimensional variation of amplitudes $a(x)$. This process is demonstrated in Fig. 2.5.

Fig. 2.5(a) depicts the twelfth Eigen-shape of a plate: the dark zones represent the maximum deformations from the state of equilibrium; the white zones indicate areas that do not oscillate at this resonance frequency. Fig. 2.5(b) illustrates 500 horizontal one-dimensional moiré gratings. After setting $k = 0.0025$ and $b = 0.0075$ for further calculations, the initial range of true values $[-1,1]$ is changed to the required range of amplitudes $[0.005,0.01]$.

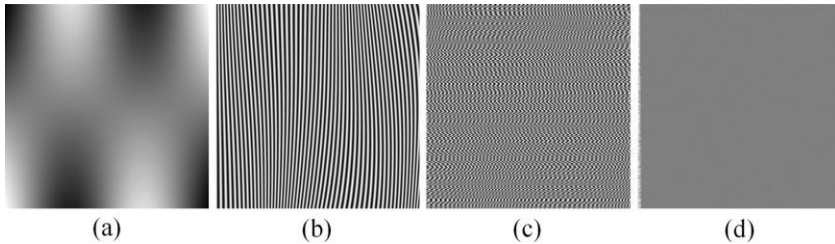


Fig. 2.5. Harmonic oscillations according to the 12th Eigen-mode of a free rectangular plate produce a gray two-dimensional image: part (a) shows the Eigen-shape; part (b) illustrates the stationary moiré grating (the pitch of the grating varies in the interval $\lambda = [0.013,0.026]$; $\lambda(x) = \frac{2\pi}{r_1} a(x)$); part (c) shows the cover image produced from the moiré grating; part (d) illustrates the time-averaged image when the cover image is oscillated according to 12th Eigen-mode

The functionality of such image hiding schemes based on dynamic visual cryptography is demonstrated by the following computational experiment. The secret dichotomous image is embedded into the cover image by employing the 12th Eigen-shape of the rectangular plate. The stochastic initial phase and phase regularization algorithms are employed to hide the secret. It is impossible to recognize the secret image from the cover image with the naked eye. Moreover,

³ *The results presented in this section have been published as:*
 Image hiding in time-averaged moiré gratings on finite element grids
 Vaidelys M.; Ragulskiene J.; Aleksiene S.; Ragulskis M.
 Copyright © 2015 Elsevier Inc.

the secret image can only become visible when the deformable encoded image is oscillated according to the Eigen-mode, which was used to encode the secret.

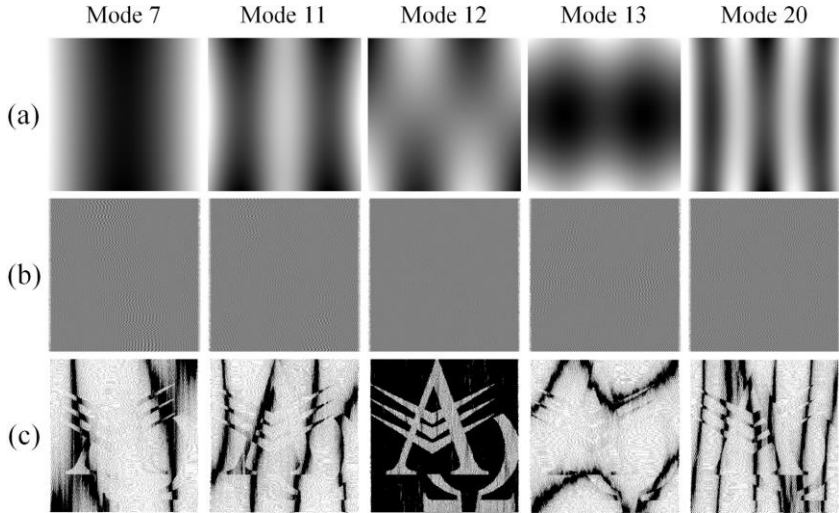


Fig. 2.6. The Eigen-mode serves as the key for visual decryption of the cover image. Line (a) shows different Eigen-shapes; line (b) – the time-averaged images; line (c) – the highlighted time-averaged images

In other words, the Eigen-mode can be considered as the key of the visual decoding procedure. Fig. 2.6 shows the results of visual decoding when the encoded image is oscillated according to different Eigen-modes. Image highlighting procedures [30] are used to better visualize the moiré interference fringes in time-averaged images.

2.4. Chaotic oscillations, non-deformable moiré grating

Let us consider chaotic oscillations of a non-deformable moiré grating:

$$F_t(x) = \frac{1}{2} + \frac{1}{2} \lim_{T \rightarrow \infty} \frac{1}{T} \int_0^T \left(\cos \left(\frac{2\pi}{\lambda} (x - \theta(t)) \right) \right) dt; \quad (2.15)$$

where $\theta(t)$ is a time function determining chaotic deflection from the state of equilibrium. If $\theta(t)$ is a Gaussian normal ergodic process, approximated by a discrete scalar series of normally distributed numbers with zero mean and σ variance, the time-averaged image reads [31]:

$$F_t(x) = \frac{1}{2} + \frac{1}{2} \cos \left(\frac{2\pi}{\lambda} x \right) \exp \left(-\frac{1}{2} \left(\frac{2\pi}{\lambda} A \sigma \right)^2 \right). \quad (2.16)$$

It should be mentioned that time-averaged fringes do not form at all in the case of chaotic oscillations [31].

Standard deviation of the grayscale intensity of time-averaged moiré (Eq. (2.16)) reads:

$$S(F_t(x)) = \frac{1}{\lambda} \int_0^\lambda (F_t(x) - E(F_t(x)))^2 dx = \frac{\sqrt{2}}{4} \exp\left(-\frac{1}{2} \left(\frac{2\pi}{\lambda} A\sigma\right)^2\right). \quad (2.17)$$

However, it is difficult to construct a clear physical interpretation for the replacement of a continuous chaotic function by a discrete scalar series of normally distributed numbers (though such replacement is beneficial for building theoretical relationships). Therefore we continue by assuming that $\theta(t)$ is a solution of the paradigmatic chaotic model – the Rossler system [32]:

$$\begin{cases} \frac{dx_1}{dt} = -x_2 - x_3, \\ \frac{dx_2}{dt} = x_1 + ax_2, \\ \frac{dx_3}{dt} = bx_1 - cx_3 + x_1x_3; \end{cases} \quad (2.18)$$

where x_1, x_2, x_3 are functions of time t ; a, b, c are constant parameters. The Rossler system exhibits stationary, periodic, quasiperiodic, and chaotic behavior at different values of the parameters.

2.4.1. Linear shape function of $a(x)$

Let us consider a deformable one-dimensional moiré grating with a constant pitch in the state of equilibrium $\lambda = 0.2$. Let us assume that the left side of the moiré grating is fixed and the right side is oscillating according to the chaotic time function $g(t) = Ax_1(t)$. Moreover, let the shape function of in-plane oscillations be linear: $a(x) = x$. Then,

$$F(x, t) = \frac{1}{2} + \frac{1}{2} \cos\left(\frac{2\pi}{\lambda} \cdot \frac{x}{1 + Ax_1(t)}\right); \quad (2.19)$$

where the parameter A varies from 0 to 0.3 (analogously as in Figure 2.7). The resulting time-averaged images are illustrated in Figure 2.7(c).

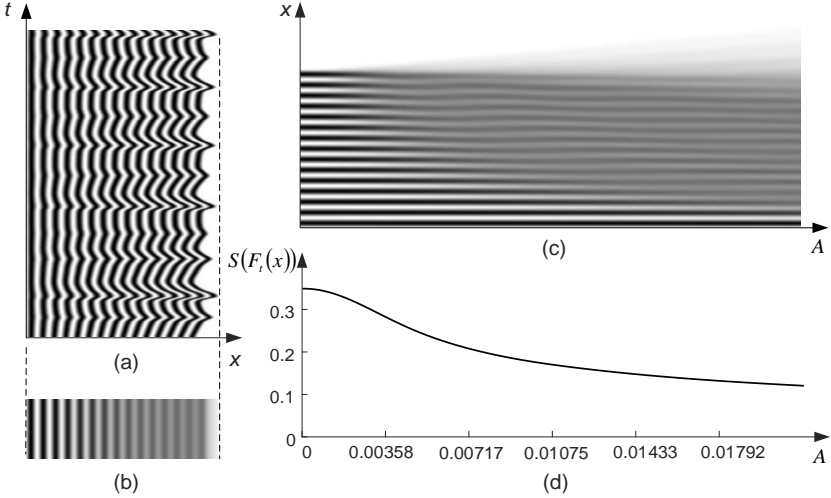


Fig. 2.7. Time-averaged image of the deformable one-dimensional moiré grating at $a(x) = x$ and $g(t) = Ax_1(t)$: (a) chaotic motion of one-dimensional moiré grating at $A = 0.005$; (b) time-averaged image of part (a); (c) one-dimensional time-averaged moiré grating at different values of A ; (d) standard deviation of time-averaged one-dimensional images

2.4.2. Nonlinear shape function $a(x)$

Let us analyze the case when the shape function describing the oscillation mode of a deformable one-dimensional body is nonlinear. The argument of cosine function in Eq. (2.13) can be rearranged as follows:

$$\begin{aligned} \frac{x - (a_0 - \dot{a}_0 x_0)g(t)}{1 + \dot{a}_0 g(t)} &= \\ &= (x - (a_0 - \dot{a}_0 x_0)g(t))(1 - \dot{a}_0 g(t)) + O(\dot{a}_0^2). \end{aligned} \quad (2.20)$$

Let us denote $a_0 + \dot{a}_0(x - x_0) = \bar{a}(x)$. Then the deformed moiré grating reads:

$$\begin{aligned} F(x, t) \approx \frac{1}{2} + \frac{1}{2} \cos \left(\frac{2\pi}{\lambda} (x - (a_0 - \dot{a}_0 x_0)g(t) - \dot{a}_0 x g(t) \right. \\ \left. + (a_0 - \dot{a}_0 x_0)\dot{a}_0 g^2(t)) \right) = \end{aligned} \quad (2.21)$$

$$\begin{aligned}
&= \frac{1}{2} + \frac{1}{2} \cos\left(\frac{2\pi}{\lambda}(x + (a_0 - \dot{a}_0 x_0)\dot{a}_0 g^2(t))\right) \cos\left(\frac{2\pi}{\lambda}\bar{a}(x)g(t)\right) + \\
&\quad + \frac{1}{2} \sin\left(\frac{2\pi}{\lambda}\cdot(x + (a_0 - \dot{a}_0 x_0)\dot{a}_0 g^2(t))\right) \sin\left(\frac{2\pi}{\lambda}\cdot\bar{a}(x)g(t)\right).
\end{aligned}$$

Time averaging of Eq. (2.21) yields:

$$\begin{aligned}
F_t(x) &= \lim_{T \rightarrow \infty} \frac{1}{T} \int_0^T F(x, t) dt = \frac{1}{2} + \\
&+ \frac{1}{2} \lim_{T \rightarrow \infty} \frac{1}{T} \int_0^T \cos\left(\frac{2\pi}{\lambda}\cdot(x + (a_0 - \dot{a}_0 x_0)\dot{a}_0 g^2(t))\right) \cos\left(\frac{2\pi}{\lambda}\cdot\bar{a}(x)g(t)\right) dt + \\
&\quad + \frac{1}{2} \lim_{T \rightarrow \infty} \frac{1}{T} \int_0^T \sin\left(\frac{2\pi}{\lambda}\cdot(x + (a_0 - \dot{a}_0 x_0)\dot{a}_0 g^2(t))\right) \sin\left(\frac{2\pi}{\lambda}\cdot\bar{a}(x)g(t)\right) dt.
\end{aligned} \tag{2.22}$$

If the time function $g(t)$ is the Gaussian normal ergodic process, it can be approximated by a discrete scalar series of normally distributed numbers with zero mean and σ^2 variance:

$$g_i \sim N(0, \sigma), \quad i = 1, 2, \dots, k. \tag{2.23}$$

However, if g_i are normally distributed numbers with zero mean and σ^2 variance, then g_i^2 are distributed according to chi squared distribution ($g_i^2 \sim \chi^2(1)$) and $Eg_i^2 = \sigma^2$ [33]. Now, Eq. (2.21) can be rearranged by replacing σ^2 by $g^2(t)$:

$$F_t(x) \approx \frac{1}{2} + \frac{1}{2} \cos\left(\frac{2\pi}{\lambda}(x + (a_0 - \dot{a}_0 x_0)\dot{a}_0 \sigma^2)\right) \exp\left(-\frac{1}{2}\left(\frac{2\pi}{\lambda}\cdot\bar{a}(x)\sigma\right)^2\right). \tag{2.24}$$

The obtained relationship in Eq. (2.24) corresponds well with Eq. (2.16). It is clear that in the case of stochastic oscillations time-averaged fringes do not form at all. Higher variance and/or higher values of maximum deflections yield more intensive blur. However, this relationship is only approximate since it was derived under the assumptions that $g^2(t)$ can be replaced by σ^2 .

2.4.3. The information capacity of the image hiding scheme

Let us take four different sizes of the square elements. (Fig. 2.8). The pitch of the moiré grating is variable in the observation window. Nevertheless, we use the mean value of the pitch and construct four computational experiments. Fig 2.8(a) represents a square element embedded in the center of the cover image; the length of the side of this element is equal to $0.25\bar{\lambda}$ ($\bar{\lambda}$ is the mean pitch in the observation window). The top image is the time-averaged cover image performing

chaotic oscillations according to the predefined shape function. The bottom image is the contrast enhanced time-averaged cover image.

Analogously, computational experiments with a square element with the side length equal to $0.5\bar{\lambda}$ is illustrated in Fig. 2.8(b), $\bar{\lambda}$ – in Fig. 2.8(c) and $2\bar{\lambda}$ – in Fig. 2.8(d). Thus, the minimum size of an element to be interpretable in the time-averaged image must be not smaller than a half of the mean pitch (Fig. 2.8).

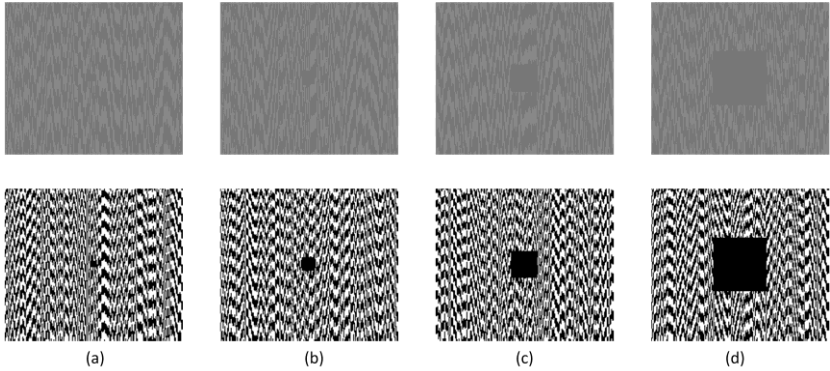


Fig. 2.8. The information capacity of the image hiding scheme. Figures in the top row represent time-averaged images of a deformable moiré grating performing chaotic oscillations; figures in the bottom row – respective contrast-enhanced images. The length of the side of the square secret element is $0.25\bar{\lambda}$ (part (a)); $0.5\bar{\lambda}$ (part (b)); $\bar{\lambda}$ (part (c)) and $2\bar{\lambda}$ (part (d)), where $\bar{\lambda}$ is the mean pitch in the observation window

2.4.4. The security of the image hiding scheme

As mentioned previously, the proposed image hiding scheme belongs to the class of visual cryptography techniques – special algorithms are required to encode the image, but decoding does not require a computational device and is completely visual. Classical visual cryptography schemes are based on the splitting of the secret image into several shares. Each share separately is cryptographically secure – the secret is leaked when all shares are accurately overlaid on top of each other. However, the secret image is not split into shares in this dissertation. Only one cover image is used, and the secret is leaked in the time-averaged image.

Let us consider a simplified situation when shape functions are constant in the whole window of observation. Such situation would result in deformable moiré gratings with constant pitches in the state of equilibrium. Let the pitch in the area occupied by the secret image be λ_s , and the pitch in the background – λ_b .

It is clear that pitches λ_s and λ_b cannot differ significantly – otherwise the encoded secret could be observed with a naked eye in the static cover image. On

the other hand, the difference between λ_s and λ_b should ensure a sufficient contrast between the secret and the background in the time-averaged image. Note that vibrations of the deformable cover image are chaotic. Thus, the standard deviation of the grayscale color around 0.5 in the time-averaged image is $\sigma_s = \frac{\sqrt{2}}{4} \exp\left(-\frac{1}{2}\left(\frac{2\pi}{\lambda_s}A\sigma\right)^2\right)$ in the zone occupied by the secret, and $\sigma_b = \frac{\sqrt{2}}{4} \exp\left(-\frac{1}{2}\left(\frac{2\pi}{\lambda_b}A\sigma\right)^2\right)$ in the background (Eq. (2.17)).

The secret is leaked when a sufficient contrast between σ_s and σ_b is obtained in the time-averaged image. Assuming that time-averaged moiré fringes become almost fully developed in the regions occupied by the secret ($\sigma_s = \varepsilon$, where ε is a small positive number), the standard deviation of the background should be as large as possible: $|\sigma_b - \sigma_s| = |\sigma_b - \varepsilon| \geq \delta$. Note that $\lambda_s = \frac{\sqrt{2}\pi A\sigma}{\sqrt{-\ln(2\sqrt{2}\varepsilon)}}$ (because $\sigma_s = \varepsilon$). Therefore, the following inequality must hold true when $\sigma_b > \sigma_s$:

$$\lambda_b \geq \frac{\sqrt{2}\pi A\sigma}{\sqrt{-\ln(2\sqrt{2}(\varepsilon+\delta))}}. \quad (2.25)$$

Analogously, when $\sigma_b < \sigma_s$:

$$\lambda_b \leq \frac{\sqrt{2}\pi A\sigma}{\sqrt{-\ln(2\sqrt{2}(\varepsilon-\delta))}}. \quad (2.26)$$

Graphical interpretations of these inequalities are illustrated in Fig. 2.9. This is a standard optimization problem with constraints – find max δ (maximum difference between contrasts in the time-averaged image) at a minimum difference between λ_s and λ_b (minimum differences of pitches in the static cover image). The Pareto optimal frontier is illustrated in Fig. 2.9 by a thick solid line. Thus, if ε is set to 0.05, λ_s is 3.18 mm, the difference $|\sigma_b - \sigma_s|$ should be not smaller than 0.1, then λ_b must be not smaller than 4.8 mm (Fig. 2.9).

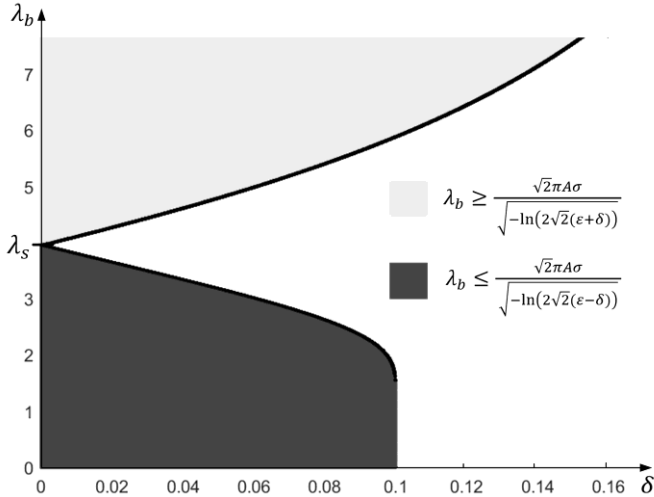


Fig. 2.9. Graphical interpretations of inequalities Eqs. 2.25 and 2.26 at $\varepsilon = 0.05$, $A = 1$, $\sigma = 1$ (thick solid line stands for the Pareto optimal frontier)

2.5. Conclusions of the second chapter

1. Secure encryption and successful decryption of the secret information are based on the proper selection of parameters of the moiré grating. Therefore, a methodology that allows the selection of optimal parameters of the moiré grating in both harmonic and chaotic oscillations has been proposed. The pitch of the secret information must ensure a uniformly grey secret area in a time-averaged image (the standard deviation in this area is zero). The background pitch must guarantee a sufficiently high standard deviation in the time-averaged image. The optimal selection of a pair of moiré grating pitches ensures a sufficient contrast of the decoded image, as well as the fact that secret information is invisible in the static cover image.
2. An image coding scheme has been proposed when the variable-pitch moiré grating oscillates according to a particular Eigen-shape. The secret information is decoded in a form of time-averaged interference moiré fringes when the encoded image is oscillated according to the same Eigen-shape as the one encoded. The efficiency of the described scheme is illustrated by numerical examples that employ the finite element method.
3. A dynamic visual cryptographic scheme which uses Ronchi-type gratings and triangular wave-form functions has been developed.
4. An image coding scheme for image hiding in stochastic deformable and chaotically vibrating moiré gratings has been proposed. The secret image

is embedded into a stationary moiré grating in such a way that secret information becomes visible in the time-averaged image when the deformable body oscillates chaotically according to a particular Eigen-shape. Although in the case of chaotic oscillations the averaged interference fringes do not form, the secret image is decoded due to the difference of gray levels in the background and secret zone in the time-averaged image.

3. TWO-DIMENSIONAL MOIRÉ GRATINGS, NON-DEFORMABLE BODY

3.1 Two-dimensional cross-gratings. Elliptic oscillations ⁴

A static two-dimensional cross-grating is described by:

$$F_2(x, y) = \frac{1}{2} + \frac{1}{2} \cos\left(\frac{2\pi}{\lambda} x\right) \cos\left(\frac{2\pi}{\mu} y\right), \quad (3.1)$$

where λ – is the pitch of the grating in the horizontal direction; μ – is the pitch in the vertical direction.

Let us assume that the deflection of a two-dimensional cross-grating around the state of equilibrium is elliptic and the radiuses of the ellipse are a and b ; then elementary trigonometric manipulation yields:

$$\lim_{T \rightarrow \infty} \frac{1}{T} \int_0^T F_2(x - a \sin t, y - b \cos t) dt = \frac{1}{2} + \frac{1}{2} \cos\left(\frac{2\pi}{\lambda} x\right) \cos\left(\frac{2\pi}{\mu} y\right) J_0(M), \quad (3.2)$$

where

$$M = \sqrt{\left(\frac{2\pi}{\lambda} a\right)^2 + \left(\frac{2\pi}{\mu} b\right)^2}; \varphi = \arctan\left(\frac{b\lambda}{a\mu}\right). \quad (3.3)$$

Thus, the time-averaged image becomes uniformly gray when the following equality holds true:

$$\left(\frac{2\pi}{\lambda} a\right)^2 + \left(\frac{2\pi}{\mu} b\right)^2 = (r_i)^2; i = 1, 2, \dots \quad (3.4)$$

If $a = b = A$, then Eq. (3.4) reduces to an explicit relationship between λ and μ :

⁴ The results presented in this section have been published as:

Image hiding scheme based on time-averaged elliptic oscillations

Saunoriene L., Aleksiene S.; Maskeliūnas R.; Ragulskis M.

Copyright © 2017 Elsevier B.V.

$$\lambda = \frac{1}{\sqrt{\left(\frac{r_i}{2\pi A}\right)^2 - \frac{1}{\mu^2}}}; \mu > \frac{2\pi A}{r_i}; i = 1, 2, \dots \quad (3.5)$$

A graphical representation of Eq. (3.5) is shown in Figure 3.1.

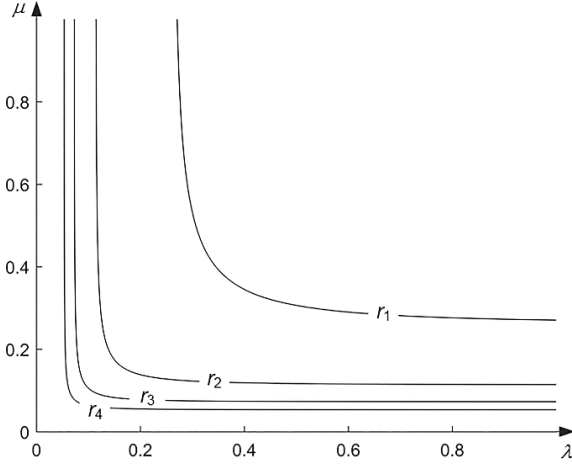


Fig. 3.1. The relationship between grating parameters λ and μ at $A = 0.1$; different curves correspond to the different values of r_i , $i = 1, 2, 3, 4$

3.2. Hiding secret in two-dimensional cross-gratings

As mentioned previously, all image hiding schemes based on dynamic visual cryptography are not cryptographically secure. The main requirement is that the secret image should not be leaked from the stationary cover image with a naked eye. Therefore, the optical security of the proposed image hiding scheme can be improved by adding random noise to the value δ .

Fig. 3.2 illustrates the implementation of an image hiding technique based on elliptic oscillations. The secret image is assumed to comprise numbers “1 2 3” and letters “A B C”. The width of the alphanumerical symbols is selected to be equal to a half of the pitch of the cross-grating in the background, which corresponds to the minimal size of the embedded square-shaped object into a stochastic moiré grating for unidirectional decoding [27].

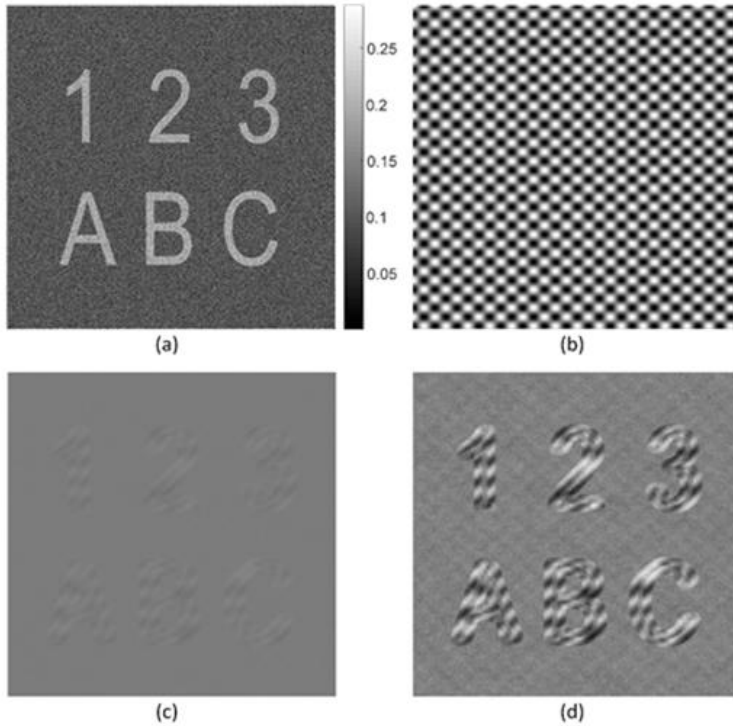


Fig. 3.2. Image hiding scheme based on elliptic oscillations: (a) values of $\delta(x, y)$ corresponding to the stationary secret image; (b) the stationary cover image at $\lambda = 0.8$, $\mu = 0.68$ (a naked eye cannot interpret the embedded secret); (c) the time-averaged image of the cover image performing elliptic oscillations at $a = 0.25$, $b = 0.15$; (d) the contrast enhancement of the time-averaged image produces clear contours of the secret image

Fig. 3.2(a) shows the values of δ used to the encode of the secret. The cover image is constructed as a deformed two-dimensional cross-grating (Fig. 3.2(b)). We consider the image is 12×12 rectangle, with pitches of two-dimensional grating $\lambda = 0.8$ and $\mu = 0.68$. It is clear that the secret information cannot be leaked with a naked eye from the cover image (Fig. 3.2(b)). The decrypted image is obtained by oscillating the cover image elliptically with amplitudes equal to $a = 0.25$ and $b = 0.15$. As it was discussed in Section 3.1, parameters μ , a and b must correspond to the relationship Eq. (3.4) in order to produce time-averaged moiré fringes. The original and contrast enhanced time-averaged images are presented in Fig. 3.2(c) and 3.2(d). Note that the size of the decrypted symbols in the time averaged image (Fig. 3.2(d)) is larger compared to the size of the encoded symbols (Fig. 3.2(a)). This is due to elliptic oscillations – the boundaries of the

symbols are blurred. The larger are the radiuses of the ellipse, the wider are the blurred boundaries.

The information capacity of the proposed scheme (the quantity of secret information that can be embedded into the cover image) is not worse than the capacity of the scheme described in.

3.3. An experimental setup for decoding the encrypted images in the case of a two-dimensional moire grating

An experimental encrypted image decoding setup (Fig. 3.3) consists of a computer (1), a cable-connected digital camera (2), and a digitally controlled table (3) with an encrypted image (4) attached to it.

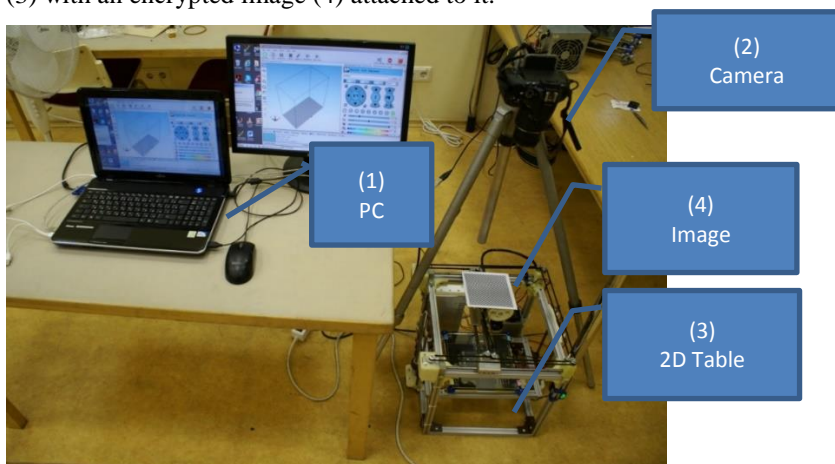


Fig. 3.3. A photo of the experimental setup

In the plane of the movement, a point (Fig. 3.4.) is placed in the center of the image. This point determines the line of motion trajectory, when the image moves. The experiment is performed primarily by determining the rotation of the stepper motors in the computer program relative to each other within a predetermined time by the predetermined parameters. A digital camera is attached above the table with the photo, the brightness is determined and the exposure time is set (in this case, 2 sec.).

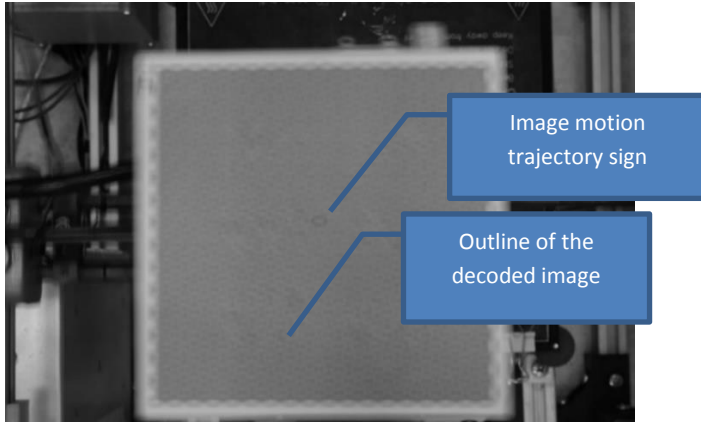


Fig. 3.4. Decoded, time-averaged image trajectory in plane with respect to x and y axes. Exposure time $T = 2$ sec; the displacement on the x axis is 3 mm; the displacement on the y axis is 5 mm

3.4. Conclusions of the third chapter

1. The image coding scheme based on elliptic oscillations has been proposed. The image is encoded by employing a two-dimensional moiré grating. The secret image appears in a form of time-averaged interference fringes, when the encoded image is oscillated according to an elliptical law of motion.
2. The essential difference between image hiding schemes based on unidirectional oscillations and elliptic oscillations is the secret embedding algorithm. One-dimensional rows (columns) can be randomly mixed in image hiding schemes based on unidirectional oscillations. However, this random mixing of phases cannot be applied to elliptic oscillations. Therefore, a new secret image hiding technique has been proposed to ensure effective optical decoding of the secret.
3. An image encoding scheme has been proposed, allowing to optically record amplitudes of angular oscillations. This scheme is based on the formation of time-averaged interference fringes in angular moiré gratings.
4. Experimental setups have been created and real experiments have been performed in case of two-dimensional cross-gratings and circular moiré gratings.

GENERAL CONCLUSIONS

1. A dynamic visual cryptographic scheme for deformable moiré gratings has been developed. This scheme allows the implementation of a black-

and-white image visual hiding scheme on the surfaces of deformable bodies defined by finite elements. This, in turn, provides the possibility of applying these schemes to the optical control of micro-opto-electromechanical systems.

2. A dynamic visual cryptographic scheme in chaotically oscillating deformable moiré gratings has been developed. This makes it possible to adapt these schemes to optical control of nonlinear systems.
3. Two dynamic visual cryptographic schemes for two-dimensional moiré gratings (for elliptical oscillations and a circular moiré grating) have been developed. This allows a significant expansion of the scope of dynamic visual cryptography for complex engineering systems. Optical setups for the experimental validation of the schemes have been created.

REFERENCES

1. Laurutis, V., G. Daunys, and R. Zemblys, *Quantitative analysis of catch-up saccades executed during two-dimensional smooth pursuit*. *Elektronika ir Elektrotechnika*, 2010. **98**(2): p. 83-86.
2. Palevicius, P. and M. Ragulskis, *Image communication scheme based on dynamic visual cryptography and computer generated holography*. *Optics Communications*, 2015. **335**: p. 161-167.
3. Sharpe, W.N., *Springer handbook of experimental solid mechanics*. 2008: Springer Science & Business Media.
4. Paturski, K., *Handbook of the moiré fringe technique*. 1993: Elsevier Sci. Publ.
5. Atluri, S. and A. Kobayashi, *Handbook on experimental mechanics*. 1993, Prentice-Hall.
6. Li, F.-C. and A. Kishen, *Deciphering dentin tissue biomechanics using digital moiré interferometry: A narrative review*. *Optics and Lasers in Engineering*, 2018. **107**: p. 273-280.
7. Lim, H., et al., *Residual microstrain in root dentin after canal instrumentation measured with digital moiré interferometry*. *Journal of endodontics*, 2016. **42**(9): p. 1397-1402.
8. Rasouli, S., Y. Rajabi, and H. Sarabi, *Microlenses focal length measurement using Z-scan and parallel moiré deflectometry*. *Optics and Lasers in Engineering*, 2013. **51**(12): p. 1321-1326.
9. Meidanshahi, F.S., K. Madanipour, and B. Shokri, *Measurement of temperature and electrons density distribution of atmospheric arc plasma by moiré deflectometry technique*. *Optics and Lasers in Engineering*, 2013. **51**(4): p. 382-387.
10. Trivedi, S., J. Dhanotia, and S. Prakash, *Measurement of focal length using phase shifted moiré deflectometry*. *Optics and Lasers in Engineering*, 2013. **51**(6): p. 776-782.
11. Juste, G.L. and E.M. Benavides, *Moiré-Fourier deflectometry for local heat transfer measurement over a backward-facing step*. *International Journal of Thermal Sciences*, 2014. **77**: p. 244-251.
12. Kuroki, H., et al., *School scoliosis screening by Moiré topography—Overview for 33 years in Miyazaki Japan*. *Journal of Orthopaedic Science*, 2018.
13. Wang, J., et al., *Volume moiré tomography based on projection extraction by spatial phase shifting of double crossed gratings*. *Optics Communications*, 2018. **407**: p. 311-320.
14. Buytaert, J.A. and J.J. Dirckx, *Phase-shifting Moiré topography using optical demodulation on liquid crystal matrices*. *Optics and Lasers in Engineering*, 2010. **48**(2): p. 172-181.

15. Jiang, N. and L. Wang, *A novel strategy for quantum image steganography based on moire pattern*. International Journal of Theoretical Physics, 2015. **54**(3): p. 1021-1032.
16. Hu, J., et al., *Design and fabrication of ultrathin lighting responsive security device based on moiré imaging phenomenon*. Optics Communications, 2018. **424**: p. 80-85.
17. Korkh, Y.V., et al., *Moiré pattern of artificial opal crystals investigated by acoustic scanning microscopy*. Applied Acoustics, 2018. **130**: p. 149-155.
18. Su, D. and Y. Zhu, *Scanning moiré fringe imaging by scanning transmission electron microscopy*. Ultramicroscopy, 2010. **110**(3): p. 229-233.
19. Brzezicki, M. *Designer's controlled and randomly generated moiré patterns in architecture*. in *Proceedings of Generative Art*. 2011.
20. Zhuang, Z., et al., *Moiré-reduction method for slanted-lenticular-based quasi-three-dimensional displays*. Optics Communications, 2016. **381**: p. 314-322.
21. Tang, Y., et al., *Beyond the partial light intensity imager: Eliminating Moiré patterns*. Optics Communications, 2015. **355**: p. 143-147.
22. Kong, L., G. Jin, and T. Wang, *Analysis of Moiré minimization in autostereoscopic parallax displays*. Optics express, 2013. **21**(22): p. 26068-26079.
23. Kobayashi, A.S., *Handbook of Experimental Mechanics*. 1998: Wiley-VCH Verlag GmbH. 1072.
24. Naor, M. and A. Shamir. *Visual cryptography*. in *Workshop on the Theory and Application of Cryptographic Techniques*. 1994. Springer.
25. Ragulskis, M. and A. Aleksa, *Image hiding based on time-averaging moiré*. Optics Communications, 2009. **282**(14): p. 2752-2759.
26. Petrauskiene, V., et al., *Dynamic visual cryptography for optical control of vibration generation equipment*. Optics and Lasers in Engineering, 2012. **50**(6): p. 869-876.
27. Palivonaite, R., et al., *Image hiding in time-averaged deformable moiré gratings*. Journal of Optics, 2014. **16**(2): p. 025401.
28. Ragulskis, M., L. Saunoriene, and R. Maskeliunas, *THE STRUCTURE OF MOIRÉ GRATING LINES AND ITS INFLUENCE TO TIME-AVERAGED FRINGES*. Experimental Techniques, 2009. **33**(2): p. 60-64.
29. Ragulskis, M. and Z. Navickas, *Time average geometric moiré—back to the basics*. Experimental Mechanics, 2009. **49**(4): p. 439-450.
30. Ragulskis, M., A. Aleksa, and R. Maskeliunas, *Contrast enhancement of time-averaged fringes based on moving average mapping functions*. Optics and Lasers in Engineering, 2009. **47**(7-8): p. 768-773.
31. Ragulskis, M., M.A. Sanjuan, and L. Saunoriene, *Applicability of time-average moiré techniques for chaotic oscillations*. Physical Review E, 2007. **76**(3): p. 036208.

32. Hilborn, R.C., *Chaos and nonlinear dynamics: an introduction for scientists and engineers*. 2000: Oxford University Press on Demand.
33. Rao, C.R., *The Concise Encyclopedia of Statistics* Springer-Verlag 2008.

LIST OF SCIENTIFIC PUBLICATIONS ON THE THEME OF THE DISSERTATION

Papers in Master List Journals of the institute of scientific information (ISI):

1. Lu, Guangqing; Saunorienė, Loreta; Aleksienė, Sandra; Ragulskis, Minvydas Kazys. Optical Image Hiding Based on Chaotic Vibration of Deformable Moiré Grating // Optics Communications. Amsterdam : Elsevier. ISSN 0030-4018. eISSN 1873-0310. 2018, Vol. 410, p. 457-467.
2. Saunorienė, Loreta; Aleksienė, Sandra; Maskeliūnas, Rimas; Ragulskis, Minvydas Kazys. Image hiding scheme based on time-averaged elliptic oscillations // Optics and Lasers in Engineering. Oxford : Elsevier. ISSN 0143-8166. eISSN 1873-0302. 2017, Vol. 98, p. 83-88.
3. Vaidelys, Martynas; Ragulskienė, Jūratė; Aleksienė, Sandra; Ragulskis, Minvydas Kazys. Image hiding in time-averaged moiré gratings on finite element grids // Applied mathematical modelling. New York : Elsevier. ISSN 0307-904X. 2015, vol. 39, iss. 19, spec. iss. SI, p. 5783-5790
4. Vaidelys, Martynas; Aleksienė, Sandra; Ragulskienė, Jūratė. Dynamic visual cryptography scheme on the surface of a vibrating structure // Journal of vibroengineering. Kaunas : JVE International. ISSN 1392-8716. 2015, vol. 17, iss. 8, p. 4142-4152.

Articles published in other peer-reviewed scientific publications:

1. Saunoriene, Loreta; Petrauskiene, Vilma; Aleksiene, Sandra; Ragulskiene, Jurate. Near-optimal pitch of a moiré grating in dynamic visual cryptography // Journal of vibroengineering. Kaunas: JVE International. ISSN 1392-8716. eISSN 2538-8460. 2018, vol. 20, iss. 6, p. 2504-2514.

Publications in conference proceedings:

1. Aleksienė, Sandra; Vaidelys, Martynas; Aleksa, Algimantas; Ragulskis, Minvydas Kazys. Dynamic visual cryptography on deformable finite element grids // AIP Conference proceedings : International conference of numerical analysis and applied mathematics (ICNAAM 2016). Melville, NY : AIP Publishing. ISSN 0094-243X. 2017, vol. 1863, iss. 1, article 440002, p. 1-4.
2. Lu, Guangqing; Maskeliūnas, Rimas; Aleksienė, Sandra; Peng, Wenbin. Experimental approach for optical registration of circular time-averaged moiré images // Vibroengineering Procedia : [28th international conference on vibroengineering, Beijing, China, 19-21 October, 2017]. Kaunas : JVE International. ISSN 2345-0533. 2017, Vol. 14, p. 364-367.

3. Saunorienė, Loreta; Aleksienė, Sandra; Ragulskienė, Jūratė. Near-optimal pitch of a moiré grating for image hiding applications in dynamic visual cryptography // *Vibroengineering Procedia* : [27th international conference on vibroengineering, Katowice, Poland, 26-28 September, 2017]. Kaunas : JVE International. ISSN 2345-0533. 2017, Vol. 13, p. 266-271.

INFORMATION ABOUT THE AUTHOR

Personal information:

Date of birth: 10th August, 1980.

Place of birth: Kaunas.

Education:

1998–2002 Bachelor in sciences of Applied mathematics, Faculty of Fundamental Science, Kaunas University of Technology.

2002–2004 Master in sciences of Applied mathematics, Faculty of Fundamental Science, Kaunas University of Technology.

2013–2018 Doctoral studies in physical sciences (informatics 09P) Department of Mathematical Modelling, Faculty of Mathematics and Nature Sciences.

Teaching experience:

From 2006 Lector, Department of Mathematical Modelling, Faculty of Mathematics and Natural Sciences.

REZIUMĖ

Dinamine vizualiąja kriptografija paremtos skaitinių vaizdų kodavimo schemos gali būti taikomos įvairiuose mokslo ir inžinerijos uždaviniuose. Žmogaus regos sistemos gebėjimas vidurkinti greitai svyruojančių objektų vaizdus laike gali būti taikomas regos sistemos specifinių ligų nustatymui, žmogaus nuovargio identifikavimui, techninių sistemų optinei diagnostikai [1]. Antra vertus, šios slaptų vaizdų kodavimo schemos turi gana didelį taikymo potencialą MOEMS (mikro–opto–elektromechaninėse sistemose) [2]. Tačiau, formuojant CGH (kompiuteriu generuotų hologramų) optinį fazių profilį, būtina įvertinti, kad projektavimo plokštumoje virpantis vaizdas atsispindi nuo deformuojamo MOEMS elemento. Taigi visi iki šiol pasiūlyti dinamine vizualiąja kriptografija paremti skaitinių vaizdų slėpimo algoritmai yra netinkami, kai šviesos srautas atsispindi nuo deformuojamo kūno paviršiaus. Šios disertacijos pagrindinis tikslas – sukurti teorinius pagrindus ir sukonstruoti atitinkamus algoritmus, leidžiančius modeliuoti dinaminės vizualiosios kriptografijos optinius efektus deformuojamosiose bei dvimatėse muaro gardelėse.

Tyrimo objektas

1. Dinamine vizualiąja kriptografija paremtų skaitinių vaizdų slėpimo algoritmų sudarymas deformuojamosiose harmoninėse muaro gardelėse.
2. Dinamine vizualiąja kriptografija paremtų skaitinių vaizdų slėpimo algoritmų sudarymas deformuojamosiose chaotinėse muaro gardelėse.
3. Dinamine vizualiąja kriptografija paremtų skaitinių vaizdų slėpimo algoritmų sudarymas dvimatėse kryžminėse muaro gardelėse.

Tyrimo tikslas

Sukurti dinaminės vizualiosios kriptografijos principais pagrįstas skaitinių vaizdų slėpimo metodikas deformuojamosiose bei dvimatėse muaro gardelėse.

Tyrimo uždaviniai

Darbo tikslui pasiekti yra iškelti tokie uždaviniai.

1. Sukonstruoti dinaminės vizualiosios kriptografijos schemą deformuojamosiose muaro gardelėse ir pritaikyti šią schemą skaitinių vaizdų slėpimui baigtiniais elementais aprašomose gardelėse.
2. Pritaikyti dinaminės vizualiosios kriptografijos, pagrįstos skaitinių vaizdų slėpimu, schemą chaotinių virpesių atveju.
3. Sukonstruoti skaitinių vaizdų slėpimo schemą dvimatėse kryžminėse muaro gardelėse.
4. Sukonstruoti standus pristatomų skaitinių vaizdų slėpimo algoritmų eksperimentiniam verifikavimui.

Tyrimų metodika

Deformuojamųjų dvimačių stochastinių muaro gardelių parametru nustatymo uždaviniai, slapto vaizdo kodavimo bei dekodavimo algoritmai konstruojami ir sprendžiami MATLAB programinėje aplinkoje. Baigtiniais elementais aprašomų deformuojamųjų kūnų paviršiaus dinamikos uždaviniai sprendžiami pasitelkiant COMSOL programą. Optimalūs modelių parametrai nustatomi taikant apytikslius analitinius metodus.

Darbo mokslinis naujumas ir praktinė reikšmė

1. Darbe pasiūlyti nauji dinaminės vizualinės kriptografijos metodai, kai deformuojama muaro gardelė svyruoja pagal tam tikrą tikrinę formą harmoniškai bei chaotiškai. Šių naujų metodų detalus išnagrinėjimas atveria galimybes taikyti pasiūlytus metodus mikro–opto–elektromechaninių sistemų optinei kontrolei.
2. Svarbiausias šios disertacijos mokslinio naujumo elementas yra dinaminės vizualiosios kriptografijos realizavimas dvimatėse baigtinii elementų gardelėse. Iki šiol žinomuose darbuose dinaminės vizualiosios kriptografijos principu pagrįstas vaizdų slėpimo algoritmas buvo paremtas laike vidurkintų muaro juostų formavimusi vienmatėse muaro gardelėse. Vaizdų kodavimo algoritmų pritaikymas dvimatėms gardelėms smarkiai išplečia pristatomų algoritmų taikymo sritis – tai ir sudaro šios disertacijos praktinę reikšmę.

Darbo rezultatų aprobavimas

Disertacijos tema paskelbti 8 moksliniai straipsniai, iš jų 4 straipsniai Mokslinės informacijos instituto (ISI) pagrindinio sąrašo leidiniuose su citavimo indeksu, 3 straipsniai pristatyti tarptautinėse mokslinėse konferencijose ir atspausdinti konferencijų pranešimų medžiagoje.

Disertacijos struktūra

Disertaciją sudaro įvadas, 3 pagrindiniai skyriai, išvados, literatūros šaltinių sąrašas. Disertacijos apimtis – 92 puslapiai. Disertacijos pagrindinėje dalyje yra 66 paveiksłai ir 98 šaltinių cituojamos literatūros sąrašas.

IŠVADOS

1. Sukurta dinaminės vizualiosios kriptografijos schema deformuojamosiose muaro gardelėse. Ši schema leidžia įgyvendinti juodai baltų vaizdų vizualinio slėpimo schemą baigtiniais elementais aprašomų deformuojamųjų kūnų paviršiuose. Tai, savo ruožtu, atveria galimybes taikyti šias schemas mikro–opto–elektromechaninių sistemų optinei kontrolei.

2. Sukurta dinaminės vizualiosios kriptografijos schema chaotiškai svyruojančiose deformuojamosiose muaro gardelėse. Tai leidžia pritaikyti šias schemas netiesinių sistemų optinei kontrolei.
3. Sukurtos dvi dinaminės vizualiosios kriptografijos schemos dvimatėse muaro gardelėse (elipsiniams svyravimams ir apskritiminei muaro gardelei). Tai leidžia pastebimai praplėsti dinaminės vizualiosios kriptografijos taikymo ribas sudėtingoms inžinerinėms sistemoms. Sukurti optiniai standai suformuotų schemų eksperimentiniam validavimui.

UDK 004.932.2 (043.3)

SL344. 2019-02-07, 2,25 leidyb. apsk. 1. Tiražas 50 egz.

Išleido Kauno technologijos universitetas, K. Donelaičio g. 73, 44249 Kaunas
Spausdino leidyklos „Technologija“ spaustuvė, Studentų g. 54, 51424 Kaunas